Chinese Physics B

PAPER

A 795 nm gain coupled distributed feedback semiconductor laser based on tilted waveguides*

To cite this article: De-Zheng Ma *et al* 2021 *Chinese Phys. B* **30** 050505

A 795 nm gain coupled distributed feedback semiconductor laser based on tilted waveguides*

De-Zheng Ma(马德正)[1,2], Yong-Yi Chen(陈泳屹)[1,†], Yu-Xin Lei(雷宇鑫)[1,‡], Peng Jia(贾鹏)[1,§], Feng Gao(高峰)[1,2], Yu-Gang Zeng(曾玉刚)[1], Lei Liang(梁磊)[1], Yue Song(宋悦)[1], Chun-Kao Ruan(阮春烤)[1,2], Xia Liu(刘夏)[1,2], Li Qin(秦莉)[1], Yong-Qiang Ning(宁永强)[1], and Li-Jun Wang(王立军)[1,3,4]

[1] *State key Laboratory of Luminescence and Application, Changchun Institute of Optics, Fine Mechanics and Physics, Chinese Academy of Sciences, Changchun* 130033, *China*

[2] *University of Chinese Academy of Sciences, Beijing* 100049, *China*

[3] *Peng Cheng Laboratory, Shenzhen* 518000, *China*

[4] *Academician Team Innovation Center of Hainan Province, Key Laboratory of Laser Technology and Optoelectronic Functional Materials of Hainan Province, School of Physics and Electronic Engineering of HaiNan Normal University, HaiKou* 570206, *China*

(Received 10 December 2020; revised manuscript received 9 January 2021; accepted manuscript online 13 January 2021)

The 795 nm distributed feedback lasers have great application in pumping the Rb D1 transition. In this paper, in order to realize specific 795 nm lasing, we designed tilted ridge distributed feedback lasers based on purely gain coupled effect induced by periodic current injection windows through changing the angle of the tilted ridge. The fabricated devices were cleaved into 2 mm-cavity-length, including 5 tilted angles. The peak output powers of all devices were above 30 mW. Single longitudinal mode lasing was realized in all tilted Fabry–Perot cavities using periodic current injection windows, with side mode suppression ratio over 30 dB. The total wavelength range covered 8.656 nm at 20 °C. It was disclosed theoretically and experimentally that the output powers, threshold currents, and central wavelengths of the tilted ridge purely gain coupled DFB lasers were relevant to the tilted angles. The results will be instructive for future design of DFB laser arrays with different central wavelengths.

Keywords: distributed feedback lasers, pumping rubidium atom, tilted waveguide

PACS: 42.55.Px **DOI:** 10.1088/1674-1056/abdb1d

1. Introduction

The 795 nm distributed feedback (DFB) lasers are competitive light sources for magnetometers,[1] precision gyroscopes,[2] and especially pumping the Rb D1 transition[3,4] used in rubidium atomic clocks. The pumping light source for rubidium clock needs small volume, high reliability and stability, and precise wavelength. Compared to other ways of achieving single longitudinal mode (SLM) laser output, such as V-cavity,[5] DBR,[6] and external cavity,[7–9] DFB laser has many advantages such as compact structure, stable dynamic single mode, reduced noise level, and easy integration.[10–14] However, conventional DFB laser diodes are mostly based on complicated nanoscale lithography and etching techniques together with regrowth steps.[15–18] Difficult fabrication process limits the applications in rubidium atomic clocks.

In this paper, we designed a novel tilted ridge purely gain coupled distributed feedback laser specifically at 795 nm for pumping light source used in rubidium atomic clocks. By using the simple fabrication process without nano precise grating structure or secondary epitaxial growth technology, the devices with tilted Fabry–Perot (F–P) ridges realized stable SLM laser output precisely at 795 nm through periodic current injection windows. The fabricated devices were cleaved into 2 mm-cavity-length, including 5 corresponding tilted angles 3.65°, 2.60°, 1.86°, 0.39°, 0° respectively. The peak output powers of all devices were over 30 mW, side mode suppression radios were over 30 dB, and total wavelength range covered 8.656 nm, from 789.392 nm to 798.048 nm at 20 °C. It was disclosed theoretically and experimentally that, different from conventional DFB lasers,[19–21] the output characteristics of the tilted waveguide purely gain coupled lasers were relevant to cavity reflection: the peak output powers of the devices were inversely proportional to the tilted angles, while the

*Project supported by the National Science and Technology Major Project of China (Grant Nos. 2017YFB0503100, 2018YFB0504600, 2018YFB2200300, and 2020YFB2205902), Frontier Science Key Program of the President of the Chinese Academy of Sciences (Grant No. QYZDY-SSW-JSC006), the National Natural Science Foundation of China (Grant Nos. 62090051, 62090052, 62090054, 11874353, 61935009, 61934003, 61904179, 61727822, 61805236, and 62004194), Science and Technology Development Project of Jilin Province, China (Grant Nos. 20200401069GX, 20200401062GX, 20200501007GX, 20200501008GX, and 20200501009GX), Special Scientific Research Project of Academician Innovation Platform in Hainan Province, China (Grant No. YSPTZX202034), Dawn Talent Training Program of CIOMP, and Independent Innovation Project of State Key Laboratory of Luminescence and Applications (Grant No. SKL1-Z-2020-02).

†Corresponding author. E-mail: chenyy@ciomp.ac.cn

‡Corresponding author. E-mail: leiyuxin@ciomp.ac.cn

§Corresponding author. E-mail: jiapeng@ciomp.ac.cn

threshold currents were proportional to the tilted angles.

The devices we designed have excellent output characteristics. The relationships between output characteristics and tilted angles were also discussed, which will be instructive for future design of gain coupled DFB laser arrays with different central wavelengths.

2. Structure and fabrication

A schematic diagram of the designed device epitaxy structure is shown in Fig. 1(a). The GaAs substrate is at the bottom of the structure and the active region is sandwiched between the p-AlGaAs and n-AlGaAs waveguides, a large gain contrast can be achieved by injecting current into the active region through the p-surface electrode. Figure 1(b) shows the structure of the tilted ridge lasers array schematically. The tilted angles from left to right are 3.65°, 2.60°, 1.86°, 0.39°, 0°, respectively. Schematic diagram of carrier injection into the active region through the periodic surface electrode is shown in Fig. 1(c). Figure 1(d) is the SEM diagram of the tilted ridge DFB laser with a tilted angle of 3.65°. The vertical distance between the two electrodes is 7.3 μm, the same as that of other devices with different tilted angles. Different tilted angles lead to the change of the effective grating period, so as to achieve the specific wavelength of 795 nm.

The key fabrication steps for these devices include material epitaxy, tilted ridge etching, insulation-layer deposition, periodic electrode patterning, metallization, and chip packaging. Through a series of above manufacture and process, chips with different tilted angles were obtained. Then the chips were cleaved into 2-mm-length devices, and coated on both sides, one with high-reflective (HR) films (> 99%) and the other with anti-reflective (AR) films (< 3%). After COS packaging, the devices were placed on a water-cooled plate for further tests at 20 °C.

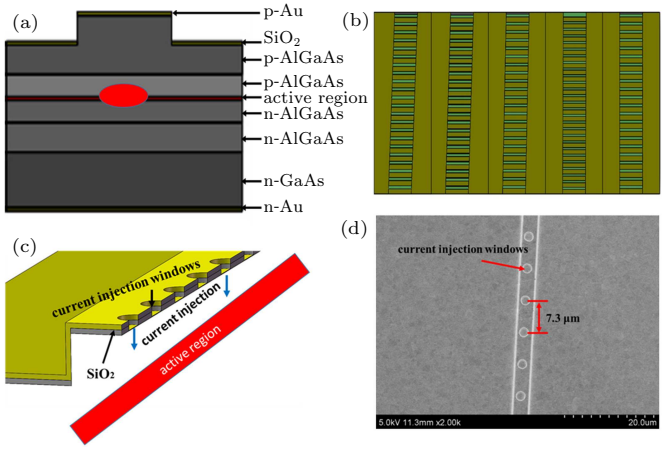

Fig. 1. (a) Schematic diagram of the designed device epitaxy structure. (b) Structure of the tilted ridge lasers array. The tilted angles from left to right are 3.65°, 2.60°, 1.86°, 0.39°, and 0°, respectively. (c) Schematic diagram of carrier injection. (d) SEM of the periodic electrode window.

3. Result and discussion

The power vs. current curves of different tilted angles are shown in Fig. 2. The peak powers of the lasers at the five tilted angles, that is 0°, 0.39°, 1.86°, 2.60°, and 3.65°, are all higher than 30 mW. The threshold currents and peak powers of the five tilted angles devices are compared, and the comparison results are shown in Fig. 3. With tilted angles increasing, the threshold currents of the devices show a gradual upward trend, but the peak powers gradually decrease. This is because with the increase of the tilted angle, the cavity surface loss of the laser increases gradually. The light returning to inside of the laser through the cavity surface cannot effectively form oscillation, causing the increase of dissipation, so the threshold current of the laser increases and the peak power decreases.

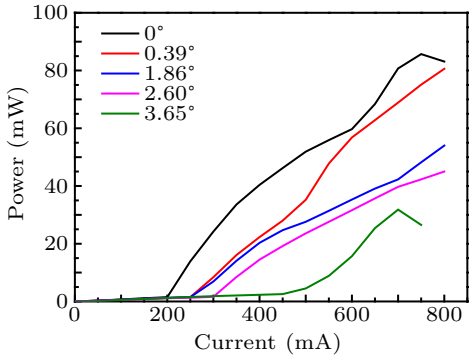

Fig. 2. Power vs. current curves of different tilted angles at 20 °C.

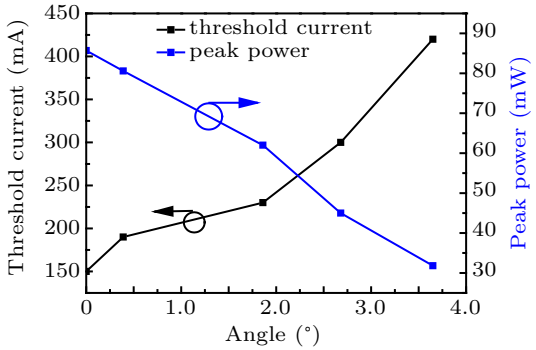

Fig. 3. Threshold currents and peak powers of devices at different tilted angles at 20 °C.

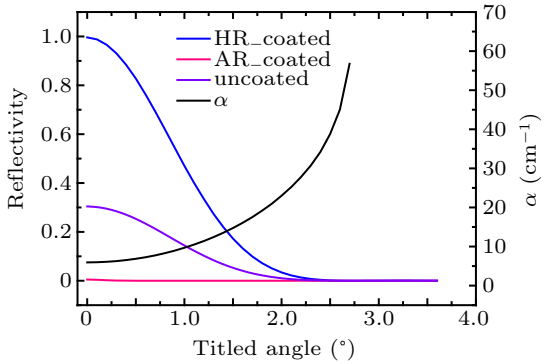

Fig. 4. The reflectance of the cavity surface varies with the tilted angles.

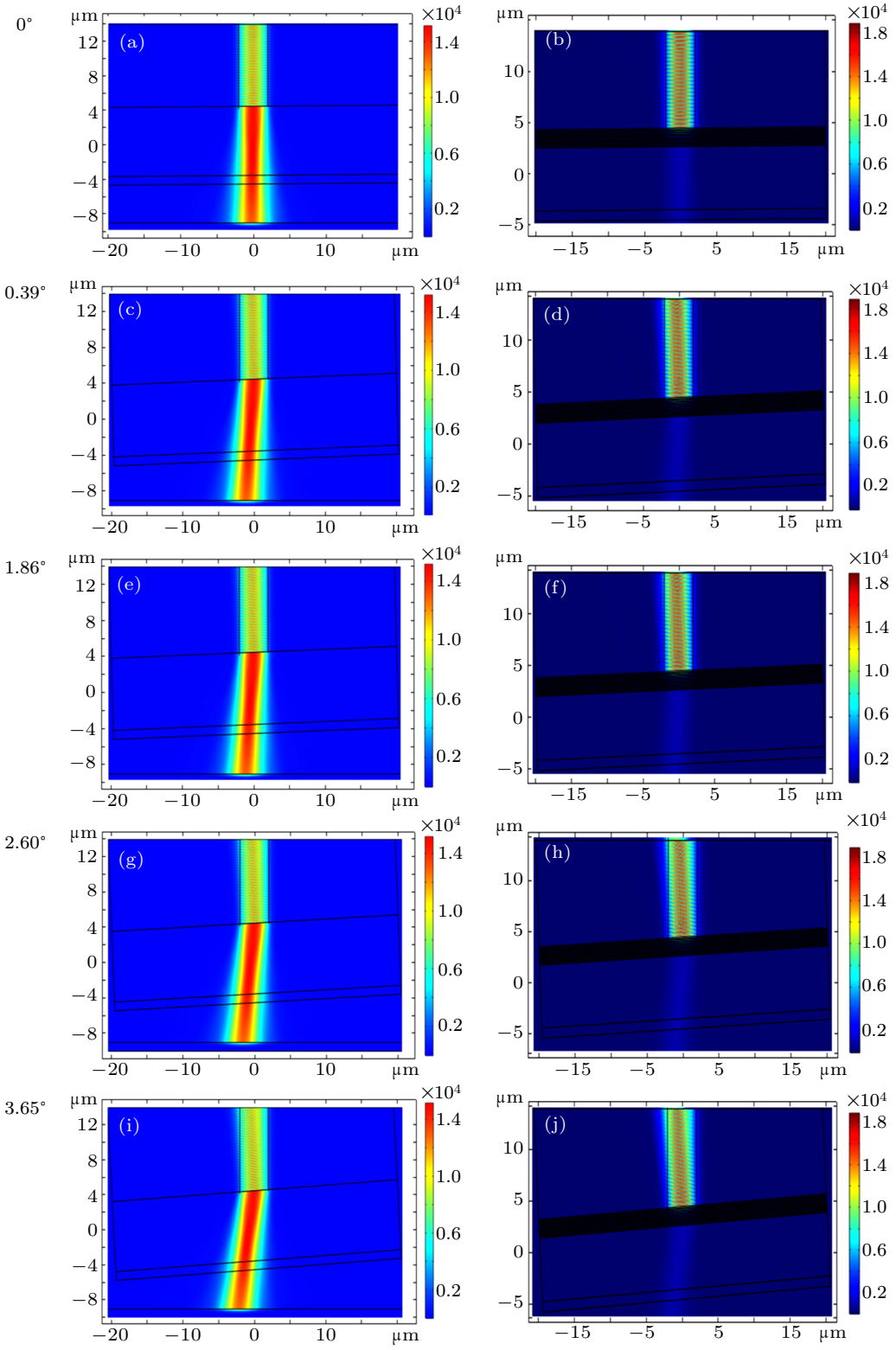

Fig. 5. The light intensity distribution on the cavity surface with tilted angles of 0°, 0.39°, 1.86°, 2.60°, and 3.65°. (a), (c), (e), (g), and (i) are uncoated surfaces. (b), (d), (f), (h), and (j) are highly reflective coating films.

We simulated the reflectivity near the cavity through the commercial software COMSOL Multiphysics to determine the influence of different tilted angles. The results of the simulations are shown in Figs. 4 and 5. Figures 5(a), 5(c), 5(e), 5(g), and 5(i) show the distribution of uncoated light intensity on the cavity surface when tilted angles are 0°, 0.39°, 1.86°, 2.60°, and 3.65°, respectively. As shown in Fig. 4, the reflectivities for the HR coated devices, uncoated devices, and AR coated devices are shown in Fig. 4 using S parameter method when the tilted angle varies from 0° to 3.65°. Utilizing the uncoated reflectivity, the cavity loss (marked as α) caused by the tilted waveguide is also calculated by the following equation:

$$\alpha = \frac{1}{2L} \ln \frac{1}{R_1 R_2}, \tag{1}$$

where L is the effective cavity length of lasers, R_1 and R_2 are the reflective indexes of the front and back cavity surfaces of lasers, respectively.

According to the simulation results, with the increase of the tilted angle, the reflectivity of the cavity surface gradually decreases and finally approaches 0, indicating that the greater the tilted angle is, the lager the mirror loss will be. This is the main reason of the enlargement of cavity loss. This gives the reason that the corresponding threshold currents will gradually increase while the peak powers will show an opposite trend.

In order to improve the output power of the tilted ridge DFB lasers, the end face of the device needs to be coated. Good HR and AR coating films will increase the power of the device,[19,22,23] which makes the device with a larger tilted angle obtain a greater gain and easily realize laser emission. By designing the corresponding coating materials, the reflectivity of HR and AR coating films is shown in Fig. 4, also the simulations of HR light intensity are shown in Figs. 5(b), 5(d), 5(f), 5(h), and 5(j), which correspond to 0°, 0.39°, 1.86°, 2.60°, and 3.65°. By comparing with Figs. 5(a), 5(c), 5(e), 5(g), and 5(i), it can be seen that most of the light is reflected by the designed highly reflective coating films, and the transmitted light intensity becomes significantly lower, so as to obtain higher power output of the device.

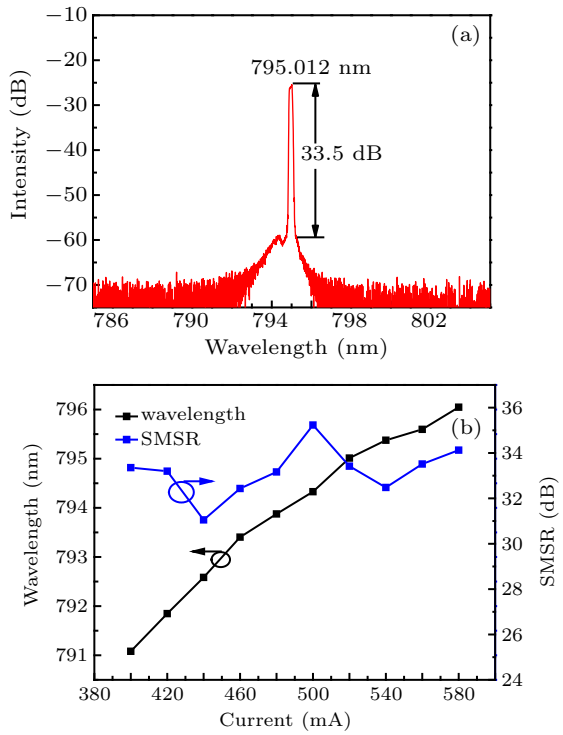

Fig. 6. (a) The 520 mA spectrum of the 0° device at 20 °C. (b) The relationship between the central wavelengths and the SMSR of the 0° device.

Then we tested the spectra of the device at 20 °C. When the injection current is 520 mA, the center wavelength is 795.012 nm. Figure 6(a) shows that the device achieved single mode operation with a SMSR of 33.5 dB. The central wavelengths increases with injection currents rising, and the relationship between the central wavelengths and the SMSR of the device and injection currents is shown in Fig. 6(b). The device maintains a good single-mode output with SMSR over 30 dB at all operating currents injection. The central wavelength of the device increases approximately uniformly and linearly with the increase of the injection current, and there is no obvious mode hopping, which shows the good output characteristics and stability of the device.

Spectra of different tilted angles corresponding to 0.39°, 1.86°, 2.60°, and 3.65° at a current of 300 mA above threshold currents respectively at 20 °C are shown in Fig. 7(a). When the tilted angle changed, as we expected, the effective grating period of the device gradually increases. The central wavelengths of the corresponding devices gradually redshift and show tunable characteristics. The wavelength tunable range of the five angles is 8.656 nm and spectra operated on all injection currents at 20 °C are shown in Fig. 7(b).

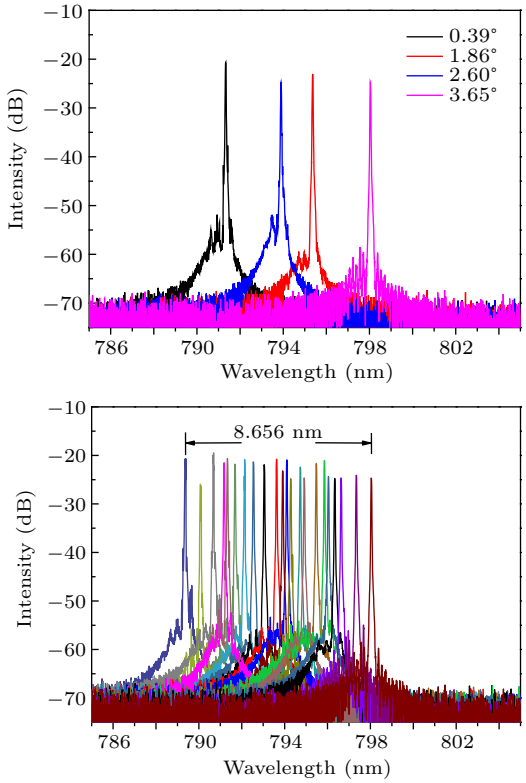

Fig. 7. (a) Spectra of different tilted angles at 20 °C. (b) Spectra of all angles at 20 °C.

We calculated the central wavelengths and current drift coefficients of the devices with different tilted angles and the results are shown in Figs. 8(a) and 8(b). It can be seen that the central wavelength of small angle devices is larger than that of large angle devices under the test current condition, because small angle devices have larger current drift coefficient. When the change in wavelength caused by injection current is greater than that caused by tilted angles, the central wavelength of small angle devices become larger.

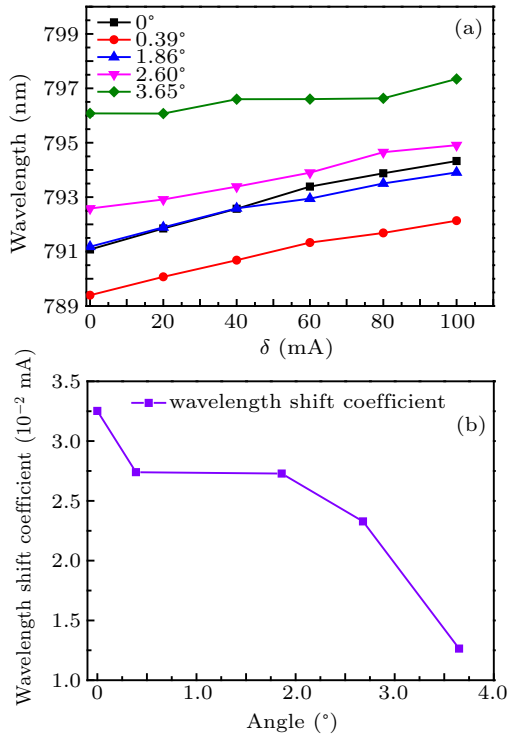

Fig. 8. (a) The central wavelengths of different tilted angles (every 100 mA). (b) Wavelength shift coefficient.

The current drift coefficient of the devices decreases with the increase of the tilted angle waveguide, that is, the application of the tilted waveguide reduces the current drift coefficient of the device, as shown in Fig. 8(b), which means, to a certain extent, the introduction of the tilted waveguide improves the wavelength stability of the device.

Due to the design of the tilted ridge, the internal distribution feedback mechanism of the device plays a leading role. The FP mode competition is weakened, consequently the spectra of the devices present a stable single mode output characteristic. The central wavelengths are related to the effective grating period of the devices. The effective period of the grating increases with the increase of the tilted angle of the ridge, which leads to the corresponding red shift of the laser wavelength. But the current drift coefficient of the devices decreases with the increase of the tilted angle waveguide, that is why the central wavelength of small angle devices is larger than that of large angle devices. The tunable output of the laser can be realized at different tilted angles and cover pumping the Rb D1 transition used in atom clocks.

4. Conclusion

Wavelength-tunable 795 nm distributed feedback lasers have great applications in pumping the Rb D1 transition. In this paper, we designed tilted ridge distributed feedback lasers, realizing a tuning range of 8.656 nm at 20 °C covering 795 nm through changing the angle of ridge. The fabricated devices were cleaved into 2 mm-cavity-length, including 5 corresponding tilted angles 3.65°, 2.60°, 1.86°, 0.39°, 0° respectively. The peak output powers of all devices were over 30 mW, SMSRs were over 30 dB, and total wavelength range covered 8.656 nm, from 789.392 nm to 798.048 nm at 20 °C. The relationship between the tilted angle and the reflectivity of the end cavity surface was obtained. Different from conventional DFB lasers, the output characteristics of the tilted waveguide lasers are relevant to cavity reflection. The peak output powers of the devices are inversely proportional to the tilted angles, while the threshold currents are proportional to the tilted angles, which is confirmed in the final test results. Also the application of the tilted waveguide reduces the current drift coefficient of the device, and the introduction of the tilted waveguide improves the wavelength stability of the device. The results will be instructive for future design of tilted waveguides.

References

[1] Budker D and Romalis M 2007 *Nat. Phys.* **3** 227
[2] Gustavson T L, Landragin A and Kasevich M A 2000 *Classical and Quantum Gravity* **17** 2385
[3] Matthey R, Affolderbach C and Mileti G 2011 *Opt. Lett.* **36** 3311
[4] Mescher M, Varghese M, Lutwak R, Serkland D K, Tepolt G, Geib K M, Leblanc J, Peake G M and Rashid A 2007 *The chip-scale atomic clock : prototype evaluation*
[5] Meng J, Xiong X, Xing H, Jin H, Zhong D, Zou L, Zhao J and He J 2017 *IEEE Photonics Technology Lett.* **29** 1035
[6] Yu L, Wang H, Lu D, Liang S, Zhang C, Pan B, Zhang L and Zhao L 2014 *IEEE Photonics Journal* **6** 1
[7] Mroziewicz B 2008 *Opto-Electronics Review* **16** 347
[8] Sato K, Kobayashi N, Namiwaka M, Yamamoto K, Kita T, Yamada H and Yamazaki H *2014 The European Conference on Optical Communication (ECOC)*, 21–25 Sept. 2014 pp. 1–3
[9] Pan G Z, Xu C, Li P T, Yang J W and Liu Z Y 2018 *Chin. Phys. B* **27** 14204
[10] Abbasi A, Abdollahi Shiramin L, Moeneclaey B, Verbist J, Yin X, Bauwelinck J, Van Thourhout D, Roelkens G and Morthier G 2018 *Journal of Lightwave Technology* **36** 252
[11] Lei Y, Chen Y, Gao F, Ma D, Jia P, Wu H, Ruan C, Liang L, Chen C, Zhang J, Qin L, Ning Y and Wang L 2019 *Appl. Opt.* **58** 6426
[12] Lei Y X, Chen Y Y, Gao F, Ma D Z, Jia P, Cheng Q, Wu H, Ruan C K, Liang L, Chen C, Zhang J, Tian J Y, Qin L, Ning Y Q and Wang L J 2019 *IEEE Photonics Journal* **11** 1
[13] Lei Y X, Chen Y Y, Gao F, Ma D Z, Jia P, Wu H, Chen C, Liang L, Zhang J, Tian J Y, Qin L, Ning Y Q and Wang L J 2019 *Opt. Commun.* **443** 150
[14] Li M, Liang S, Zhao L J and Chen M H 2013 *Chin. Phys. B* **22** 54211
[15] Guo R J, Lu J, Liu S P, Shi Y C, Zhou Y T, Chen Y T, Luan J and Chen X F 2016 *IEEE Photonics Journal* **8** 1
[16] Shi Y, Li S, Guo R, Liu R, Zhou Y and Chen X 2013 *Opt. Express* **21** 16022
[17] Brox O, Bugge F, Mogilatenko A, Luvsandamdin E, Wicht A, Wenzel H and Erbert G 2014 *Small linewidths 76x nm DFB-laser diodes with optimized two-step epitaxial gratings* (Vol. 9134) (SPIE)
[18] Brox O, Bugge F, Mogilatenko A, Luvsandamdin E, Wicht A, Wenzel H and Erbert G 2014 *Semiconductor Science and Technology* **29** 095018
[19] Chinn S R 1973 *IEEE Journal of Quantum Electronics Qe* **9** 574
[20] Gao F, Qin L, Chen Y Y, Jia P, Chen C, Cheng L W, Chen H, Liang L, Zeng Y G, Zhang X, Ning Y Q and Wang L J 2018 *IEEE Photonics Journal* **10** 1
[21] Gao F, Qin L, Chen Y Y, Jia P, Chen C, Cheng L W, Chen H, Liang L, Zeng Y G, Zhang X, Wu H, Ning Y Q and Wang L J 2018 *Opt. Commun.* **410** 936
[22] David K, Morthier G, Vankwikelberge P and Baets R 1990 *Electronics Lett.* **26** 238
[23] David K, Buus J and Baets R G 1992 *IEEE Journal of Quantum Electronics* **28** 427